ELECTRICAL ENGINEERING AND ENERGY

OPEN ACCESS

Evaluation of Magnet Demagnetization Behavior in Permanent Magnet Linear Synchronous Motors

Enes Yücel[1], Mehmet Cunkas[1], Łukasz Knypiński[2]

[1] Electrical & Electronics Engineering, Faculty of Technology, Selcuk University, Konya, Türkiye

[2] Faculty of Control, Robotics and Electrical Engineering, Poznan University of Technology, Poznan, Poland

Submitted: 2 April 2025
Accepted: 25 April 2025
Published: 30 April 2025

Corresponding author
Enes Yucel,
enes.yucel@selcuk.edu.tr

Abstract: This paper focus on investigating the demagnetization behavior of permanent magnets in Permanent Magnet Linear Synchronous Motors (PMLSMs) under varying thermal and electrical operation conditions. For this, two complementary Finite Element Method-based approaches are used. The first method utilized magnetostatic analysis to determine the B-H operating points of the magnets under worst-case conditions, allowing the identification of critical regions that tend to move away from the irreversible magnetic field. The second method employed time-domain transient analysis to monitor changes in the induced voltage under varying temperatures and stator current levels. The results revealed that increasing current and temperature significantly reduced the permanent flux density, indicating partial or complete demagnetization. Furthermore, the demagnetization thresholds were shown through safe operating area curves.

Keywords Demagnetization, Permanent Magnet Linear Synchronous Motor, Magnetic Coercivity, Safe Operating

1. Introduction

Permanent Magnet Linear Synchronous Motors (PMLSM) are widely preferred in applications that require high precision, such as laser engravers and 3D printers, thanks to their superior features such as high acceleration, direct drive structure, and precise positioning capability (Song et al., 2017; Yang et al., 2023). However, PMLSM systems are prominent not only in the field of industrial automation but also in medium- and low-speed magnetic train (maglev) applications. Halbach-type PMLSMs, whether coreless or with cores, offer significant advantages over conventional linear induction motors in traction systems due to their high synchronization capability and low operating costs (H. Wang et al., 2018).

Since permanent magnet (PM) motors operate under high temperatures and currents, permanent magnets can easily lose their magnetism. Partial demagnetization reduces the torque and power density of PM motors, while complete demagnetization leads to a complete loss of motor function. To overcome this risk, thicker or higher coercive strength magnets are often used, but this also increases the cost (Xiong et al., 2016). Therefore, the study of the phenomenon of demagnetization in PM motors is of great importance, and many studies have been conducted on this topic.

Mahmouditabar, Vahedi, and Marignetti (2023) elaborated on the basic principles of the concept of demagnetization. Four basic approaches are proposed, such as modelling of nonlinear GH characteristics, analytical evaluation of local demagnetization, and accurate experimental testing methods. Hoang et al. (2024) developed a nonlinear model for the prediction of ID in PMSMs operating under overload and high temperature. They showed that this model provides high agreement with Finite Element Analysis (FEA) and experimental results. Xiong et al. (2016) applied controlled local demagnetization on magnet samples with a specially developed test setup and compared the results with 3D FEA. Eker and Özsoy (2022) experimentally examined the effects of demagnetization failures created at different rates on motor performance and revealed decreases in torque, efficiency, and power factor. Almandoz, Gómez, Ugalde, Poza, and Escalada (2019) proposed a methodology based on finite element analysis and experimental testing, demonstrating how PM machine designs that achieve an optimal balance between cost and durability can be realized.

When the literature in this field is examined, it is seen that demagnetization is mainly considered in permanent magnet synchronous machines (PMSM). In this study, demagnetization trends in permanent magnet linear synchronous motors (PMLSM) are comprehensively investigated based on the deficiency in the literature. Two different analysis approaches are applied in the study. In the first approach, the operating points of the magnets on the B-H curve of the PMLSM under no-load conditions were determined by magnetostatic analysis, and the regions prone to demagnetization were identified. In the second approach, time-dependent transient analysis was applied to evaluate the remanent flux loss of the magnets through the induced voltage (Eq) on the q-axis at different temperature levels and various reverse current conditions. The analyses are carried out by means of FEM-based simulations and the tendency of the magnet material to demagnetize depending on temperature and current is presented in detail using the data obtained. Furthermore, based on the results of the study, safe working areas for magnet selection and motor design are defined, and design recommendations are presented for more efficient operation of PMLSM systems.

2. Demagnetization of Permanent Magnets

There are different causes of demagnetization. If the operating point is in the region where the BH curve runs linearly, there is no demagnetization. However, if the operating point approaches or falls below the "knee point" of the BH curve, partial or irreversible demagnetization may have begun. Therefore, the Remanence flux (B_r) is no longer at the initial value but at a lower value depending on the reverse magnetic field intensity to which it is exposed. This indicates that the magnet cannot maintain its initial remanent value, and some magnetic fields are lost. The operating temperature of the magnet is one of the most important factors affecting the demagnetization coercivity (H_c) and intrinsic demagnetization coercivity (H_{ci}). Magnetic coercivity is a constant material property and is the opposite of the magnetic field strength required to demagnetize a magnet completely. Figure 1 shows the standard BH curve and the point H_c and H_{ci} values corresponding to the point B_r=0 on the intrinsic BH curve. Magnetic Coercivity does not change with increasing current. Coercivity depends on the structure of the material and the operating temperature of the magnet (Üstün, 2000). There are two curves on the magnet BH graph: the intrinsic curve and the normal curve. The red one is the intrinsic curve, and the blue one is the normal curve. The yellow line represents the load line. H_a is the strength of the external magnetic field acting on the magnet. Below the knee point, the magnet loses its magnetizing property.

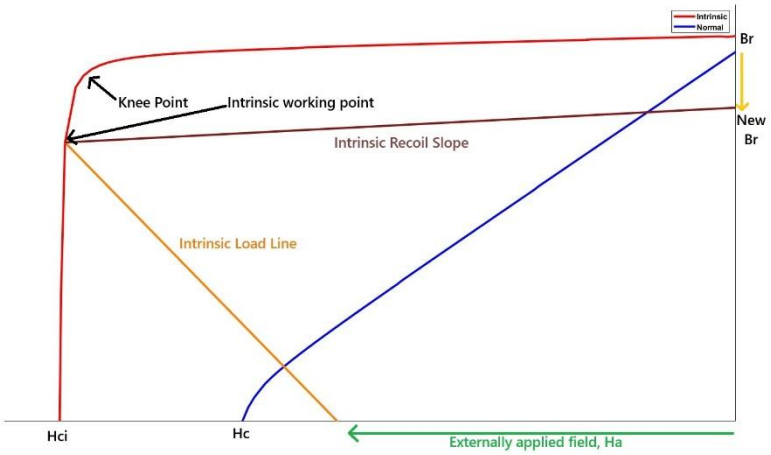

Figure 1 BH Characteristics and demagnetization behavior of sample magnet

Temperature increase and inductive reaction are the leading causes of demagnetization. However, mechanical stresses and eddy currents can also cause magnets to lose their magnetism (S. Wang et al., 2025). One of the most destructive magnetization effects in motors is the Back EMF value, which occurs due to short-circuit currents when the motor rotates at synchronous speed (Hanselman, 2003). In this study, detailed analyses were carried out on the permanent magnet mounted in runner of a designed PMLSM. The investigations were carried out to reveal the demagnetization tendencies that the magnet may be exposed to under high reverse currents and temperature increases under worst-case conditions. Comprehensive simulations were carried out using the FEA. The changes in the flux density (B) value during the demagnetization process of the magnet material were evaluated through the B-H characteristic. Since increasing operating temperature and stator current increase the risk of demagnetization of the magnet, these parameters need to be carefully monitored and limited. A magnet sample is shown in Figure 2-a, and magnetic equivalent circuit models are shown in Figure 2-b.

The magnetomotive force is the total magnetic voltage difference between the ends of the permanent magnet, and it is calculated as follows.

$$F = \emptyset_r * R_m \tag{1}$$

where $\emptyset_r$ is the magnetic flux generated by the single magnet, and R_m [A/Wb] is the total reluctance of the magnetic circuit.

Considering the electromagnetic conversion laws, the magnetomotive force can be also defined.

$$F = H * l_m \tag{2}$$

where H [A/m] is magnetic field intensity, l_m [m] is the magnetic path length of the magnet. The magnetomotive force (MMF) resulting from the passage of current through a coiled winding is defined as follows.

$$F = N * I \tag{3}$$

where N is the total number of turns, and I is the current flowing through the winding. Accordingly, the MMF statement.

$$H = \frac{N*I}{h_{pm}} \tag{4}$$

$$N * I = \emptyset_r * R_m = \frac{B_r * l_m}{\mu_0 * \mu_r} \tag{5}$$

Total flux linkage of a phase:

$$\lambda = N * \emptyset \tag{6}$$

Magnetic flux value per pole for PMLSM:

$$\emptyset = \frac{\frac{2}{\pi} B_{airgap} L_s W_s}{p} \quad (7)$$

where L_s and W_s are the width and length dimensions of the motor. Magnetic flux density is:

$$B = \mu * H \quad (8)$$

Stator reference frame d-q currents.

$$i_{d\_srf} = I_s \cos(\alpha_{Is\_srf}) \text{ and } i_{q\_srf} = I_s \sin(\alpha_{Is\_srf}) \quad (9)$$

Reference frame currents a,b,c according to the Inverse Clarke Transform.

$$i_a = i_{d\_srf}, \quad i_b = -\frac{1}{2} i_{d\_srf} + \frac{\sqrt{3}}{2} i_{q\_srf}, \quad i_c = -\frac{1}{2} i_{d\_srf} - \frac{\sqrt{3}}{2} i_{q\_srf} \quad (10)$$

In this study, the NdFeB class magnet was preferred in the single-sided PMLSM design. The main reason for this preference is that the magnet in question has a high permanent flux density and energy multiplier, allowing more compact motor designs compared to other magnets of similar power. A total of 16 magnets are placed on the secondary of the motor, with opposite poles side by side, in line with the structure shown in Figure 3. Detailed magnetic characteristics of the magnet used are presented in Table 1.

Table 1 Properties of the N38UH 150C permanent magnet material used in the design

Parameter	Type	Value	Unit
Relative permeability	Nonlinear	B-H Curve	-
Bulk conductivity	Simple	555555.5556	siemens/m
Magnetic coercivity (H_C)	Vector	-922100	A/m
Mass density of core	Simple	7500	kg/m³
Remanence flux	Simple	1.0634	T
Max. working temp.	Simple	150	℃

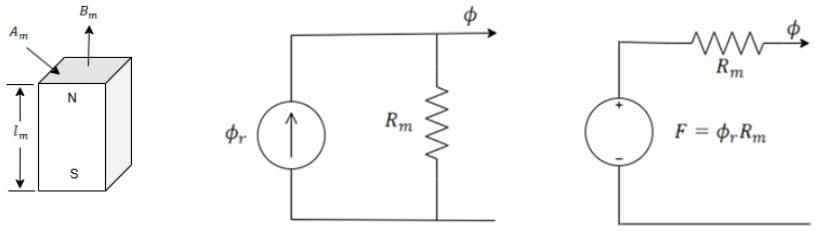

(a) (b)

Figure 2 a-) Sample of permanent magnet b-) Norton and Thevenin magnetic equivalent circuits

3. Analysis of demagnetization in PMLSM design

In this study, two methods were applied in demagnetization analysis. Firstly, demagnetization due to overload under worst-case conditions was investigated. In the analysis, the magnetic field distributions of PMLSM under worst-case conditions were obtained with a magnetostatic solvent. The operating points on the B-H curve of a selected magnet on the secondary were determined and shown in the figure. Then, demagnetization due to temperature rise was investigated. A three-phase time-dependent transient analysis was performed for a single magnet. In this context, the demagnetization tendencies of magnets with different

temperature levels under different current conditions were examined, and the effects of demagnetization were analyzed, especially considering the change in E_q value.

3.1 Analysis of demagnetization caused by overload

The B and H distributions obtained because of the no-load analysis of the magnet located in the primary of the PMLSM and marked in the circle are presented in Figure 3. When the B and H magnetic flux distributions on the PMLSM are analyzed separately, comments can be made due to the magnet-material interaction. Accordingly, it is seen that the B value is higher at the ends of the magnet and lower in the center. The reason for this is that the magnetic flux density accumulates at the ends of the magnet, and the magnetic flux starts inside the magnet and goes out from the ends. In Figure 3, the magnetic field strength is maximum in the center of the magnet as the largest MMF is formed. Towards the end, H decreases because the leakage fields become larger. Although the magnetic flux density is directed toward the ends of the magnet, the field generating power is low there because there is MMF loss at the ends, and the H (A/m) value is low. Therefore, demagnetization is easier in these regions.

In the study, analyses were carried out at various current levels using Ansys Maxwell 2D Magnetostatic solver. The type of magnet used is Arnold Magnetics N38UH 150C. The analyses were repeated for no-load ($1.I_{s\_pu}$) and loaded/loading operation state ($5.I_{s\_pu}$, $9.I_{s\_pu}$, $13.I_{s\_pu}$, $17.I_{s\_pu}$, $20.I_{s\_pu}$). The analysis was positioned along the magnet with respect to the distance axis for each parameter, and three graphs were obtained. Accordingly, Figure 4-a shows the average magnetic flux density at the magnet (B_{magnet}), Figure 4-b shows the magnetic field strength at the center of the magnet (H_{magnet}), and Figure 4-c shows the average magnetic flux density in the air gap ($B_{air\ gap}$).

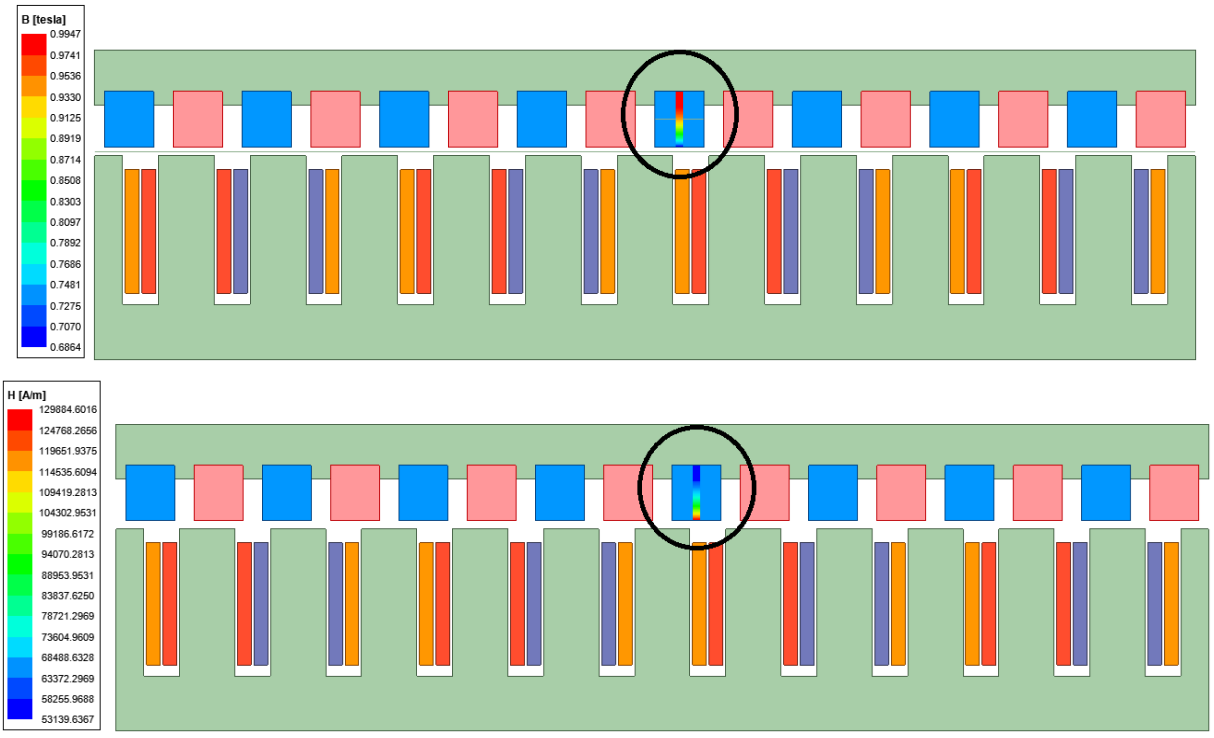

Figure 3 B and H distribution obtained from the no-load analysis

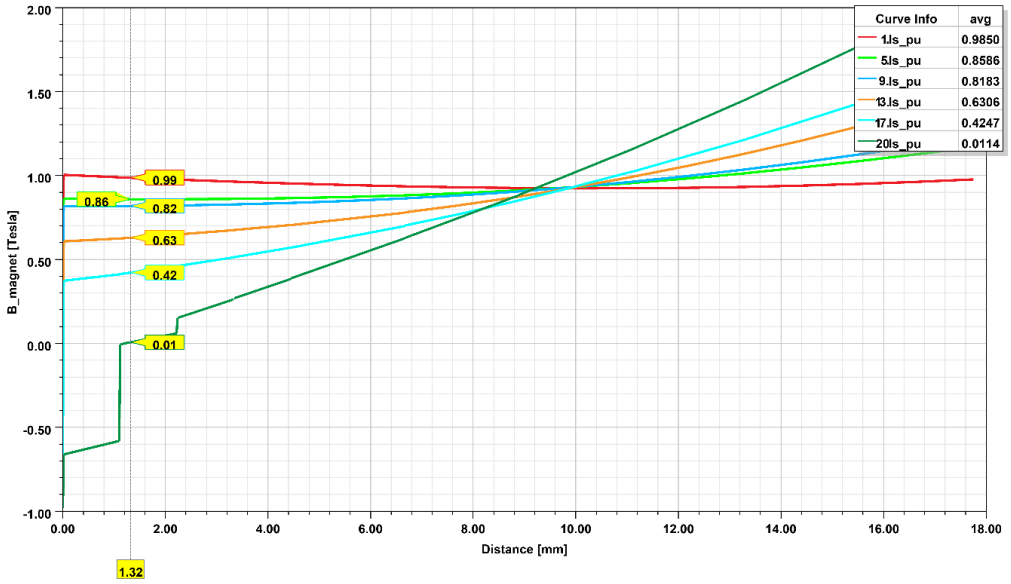
Curve Info
avg
1.Is_pu
0.9850
5.Is_pu
0.8586
9.Is_pu
0.8183
13.Is_pu
0.6306
17.Is_pu
0.4247
20Is_pu
0.0114
B_magnet [Tesla]
Distance [mm]
0.99
0.86
0.82
0.63
0.42
0.01
1.32

(a)

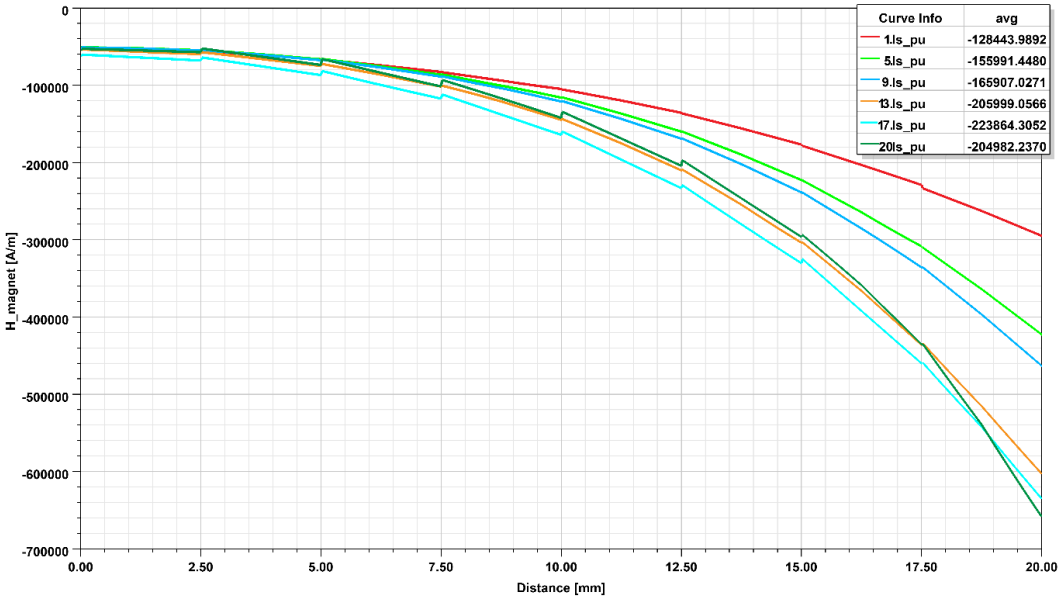
Curve Info
avg
1.Is_pu
-128443.9892
5.Is_pu
-155991.4480
9.Is_pu
-165907.0271
13.Is_pu
-205999.0566
17.Is_pu
-223864.3052
20Is_pu
-204982.2370
H_magnet [A/m]
Distance [mm]

(b)

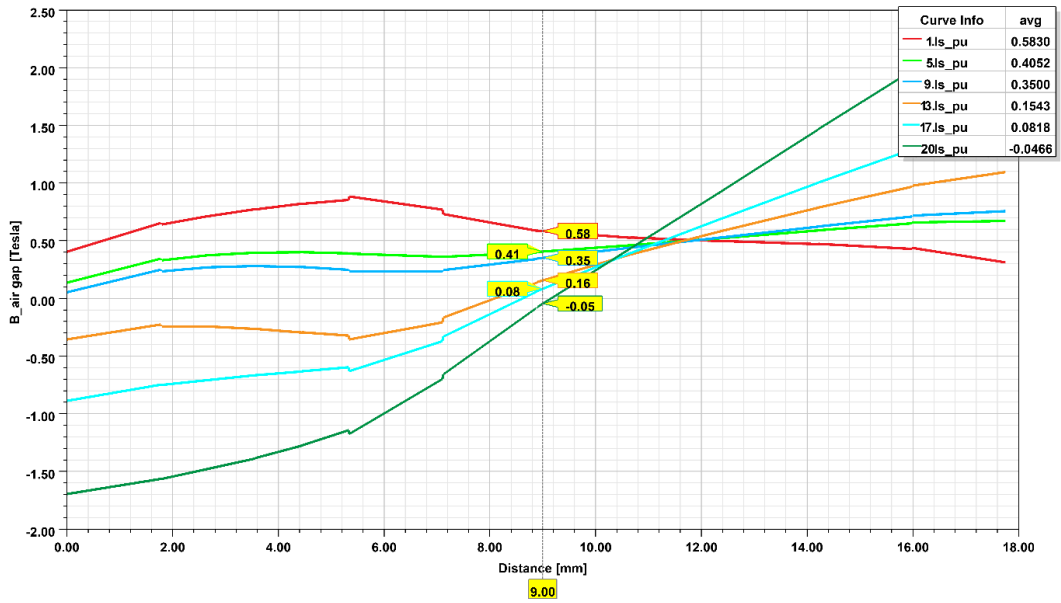

(c)

Figure 4 Results of comparison along the length of the magnet a) Average magnetic flux density b) Magnetic field intensity at the center of the magnet c) Average magnetic flux density in the air gap

While H_{magnet} value is around -128,000 A/m at no-load operation, the H value becomes more negative as the load increases, reaching -610,000 A/m at 20.I_(s_pu) current. This shows that as the reversing current passing through the stator winding increases, the reversing H value in the magnet increases and approaches the coercive force of the magnet. While $B_{magnet} = 0.99\ T$ at no-load operation, this value decreased to 0.86 T, 0.82 T, 0.63 T, 0.42 T and 0.01 T, respectively, as the current increased. Especially at $20.I_{s\_pu}$, the B_{magnet} value approaches almost zero, indicating that the magnet is severely demagnetized. The $B_{air\ gap}$ value in the air gap also decreases with the load. This decrease indicates that the magnetic field generated by the magnet is weakened by the reverse current flowing through the stator windings, and as a result, the total net magnetic flux in the air gap may decrease. This makes it difficult for the motor to operate correctly. In a motor with a loss of magnetization, the stator current must be increased to achieve the same electromagnetic torque. This creates serious problems for thermal insulation and significantly shortens the life of the motor (Gyftakis, Ab Rasid, Skarmoutsos, & Mueller, 2021).

The simulation results were utilized to determine the working points on the B-H curve of the magnet analyzed in the PMLSM. Based on the analysis, the H_{magnet} and the corresponding B_{magnet} values, measured at the center of the magnet, were identified as the working points for the specified load conditions and are presented in Figure 5.

When the graph is examined, it is observed that at low current levels, such as I_{s_pu}, the magnet still operates within the linear region. After the value, the working points move into the region where the slope of the curve decreases, approaching partial saturation or the demagnetization zone. As seen from the graph, the B_r value of the magnet is 1.06 Tesla. At the $20.I_{s\_pu}$ level, the working point drops below the knee point of the B-H curve, indicating that the magnet is significantly stressed and irreversible demagnetization may have occurred. When B_{magnet} is 0.01T, $H_{magnet} = -739{,}434\ A/m$ is -739.434 a/m, which corresponds to the intrinsic coercivity point H_{ci} where full demagnetization occurs. Therefore, it can be concluded from the graph that the magnet retains its magnetization until the reverse magnetic field reaches −739 kA/m.

Furthermore, the graph clearly illustrates how the working points approach the demagnetization region as the magnet is subjected to negative H_{ci} fields. To avoid reaching this critical limit, the MMF value can be constrained, or the magnet thickness can be increased, as indicated in Equation 6.

3.2 Analysis of demagnetization caused by temperature increase

Three-phase transient analysis was performed, and E_q was monitored for the rotor reference frame. The mathematical expression of E_q is given as:

$$E_q = \omega_e * \lambda_M \tag{11}$$

where ω_e represents the electrical angular velocity of the rotor (rad/s), and λ_M denotes the flux linkage of the magnet, which is predominantly defined along the d-axis. As can be understood from the equation, when no current is applied to the stator windings ($I_d = 0$, $I_q = 0$) under a constant electrical angular velocity, the windings do not generate any magnetic field, and all the magnetic flux in the system originates solely from the permanent magnets. Therefore, E_q is directly proportional to the magnet flux. During the analysis process, the remanent flux linkage λ_M cannot be directly measured, but E_q can be measured. Thus, demagnetization detection was carried out by tracking the E_q voltage. The simulation procedure was structured into three periods: initially, the motor was operated under no-load conditions, followed by the application of loaded operation, and finally, the system was returned to the no-load state. This approach enabled a comparative evaluation of magnet behavior before and after loading.

In the first period, when no current is applied to the system, the stator current vector angle between the stator current vector and the stator d-axis (α_{Is_srf}) is set to 90 degrees, and only the magnet-induced voltage (E_{q1}) is generated. In this condition, as illustrated in Figure 6, the magnet flux λ_M, aligned along the d-axis in the rotor reference frame, produces an E_q voltage along the q-axis. This induced voltage is designated as the reference point E_{q1} for subsequent comparative analyses.

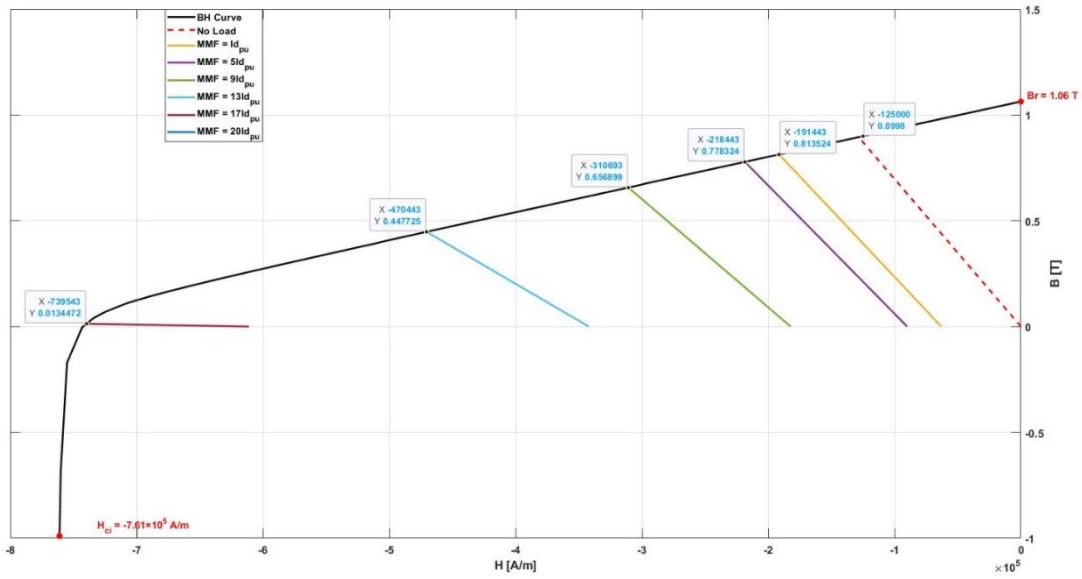

Figure 5 B-H Curve of the Magnet for Operating Points at Different Load Conditions

In the second period, as shown in Figure 7, current is applied such that the stator current vector angle α_{Is_srf} is 180 degrees in the rotor reference frame. This creates a stator magnetic field density (B_S) directly opposing the magnet flux. In this worst-case scenario for the magnets, the λ_M value weakens, resulting in a decrease in theE_q voltage. The analysis was repeated for various load conditions (1.I_{s_pu}, 5.I_{s_pu}, 9.I_{s_pu}, 13.I_{s_pu}, 17.I_{s_pu}, 20.I_{s_pu}) and for magnets with three different operating temperature classes: Arnold Magnetics N38UH 80C, Arnold Magnetics N38UH 120C, and Arnold Magnetics N38UH 150C.

In the third period, I_{s_pu} is reset to zero. During this phase, the obtained E_{q3} value is compared with E_{q1} to detect demagnetization. If $E_{q1} = E_{q3}$, it indicates that the magnet has not been permanently affected, the system has remained within the linear region of the B-H curve, and the B_r value has not changed. However, if $E_{q3} < E_{q1}$, it indicates that the magnet has undergone demagnetization and a permanent flux loss has occurred. During demagnetization, a new B_r value is formed, and this new remanent flux density is reached along the intrinsic recoil slope.

As a result of the analyses performed with these parameters, the graphs presented in Figure 8 were obtained. In the tables embedded within the graphs, the "avg." value corresponds to the voltage induced by the magnet in the coils during the first period when no current is applied. The "avg_1" value refers to the induced voltage measured during the third period after the application of high currents. Since magnets lose their energy with increasing temperature, this behavior is directly related to their demagnetization temperature. A lower operating temperature for the magnet reduces the risk of demagnetization. For most magnets, both the remanent flux density and the magnetic coercivity decrease with increasing temperature (Campbell, 1996). Simulations were repeated for three types of magnets characterized by different temperature classes (80^{0}C, 120^{0}C, and 150^{0}C). According to Figure 8a, for the low-temperature class magnet (20C), E_{q3} remains approximately equal to E_{q1} at low I_{s_pu} levels, but as the current increases, E_{q3} deviates from E_{q1}. As shown in Figure 8b, for the medium-temperature class magnet (120^{0}C), at higher I_{s_pu} levels, E_{q3} becomes significantly lower than E_{q1}, indicating the appearance of an intrinsic recoil slope. In Figure 8c, this difference is even more pronounced for the high-temperature class magnet (150C). At 20.I_{s_pu}, E_{q3} shows a substantial drop compared to E_{q1}, suggesting that the magnet has fallen below its knee-point and can no longer maintain its initial B_r value. According to the analysis, for the same I_{s_pu} level, magnets with higher operating temperatures exhibit lower E_q values and, thus, lower B_r values. FEM analysis was performed on three different magnets, and B_r values decreased gradually as the operating temperatures of the demagnetized magnets increased.

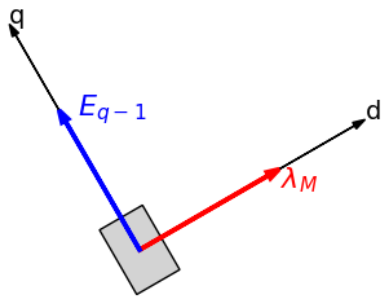

Figure 6. Vector representation of E_{q1} induced by the permanent magnet flux under no-load condition

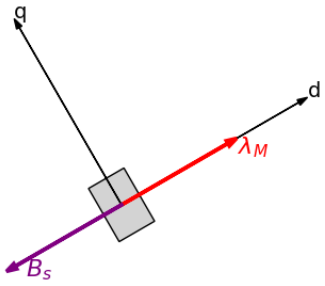

Figure 7 Vector diagram of the stator magnetic field B_S opposing the magnet flux at α_{Is_srf} = 180°

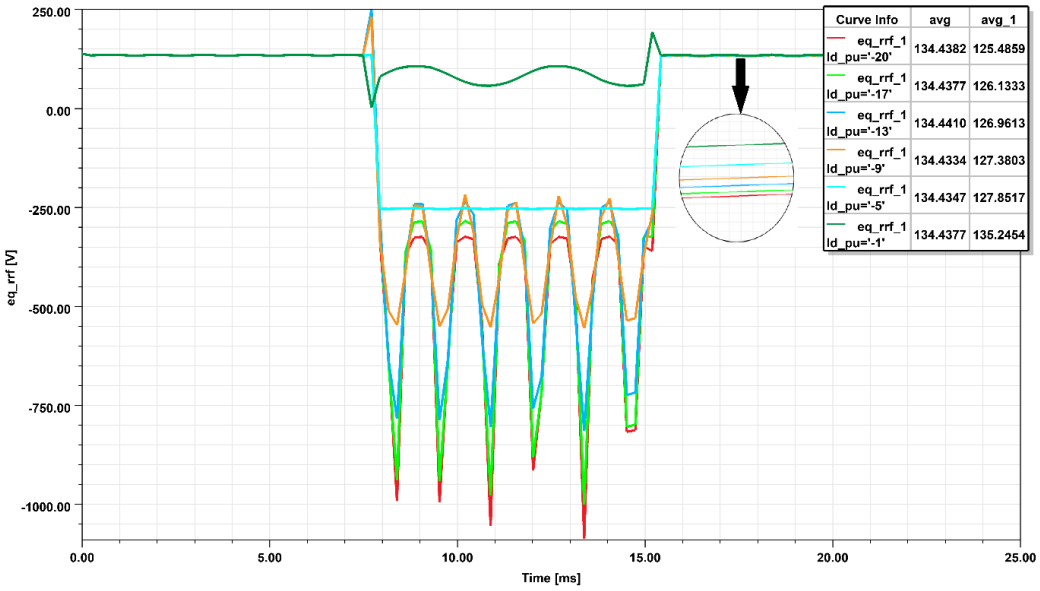

(a)

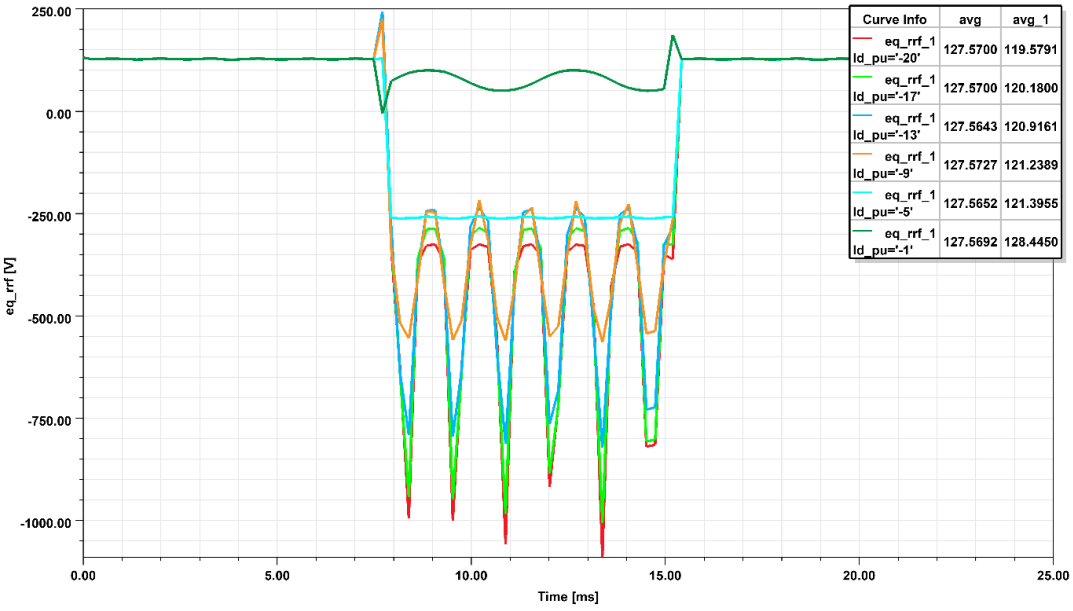

(b)

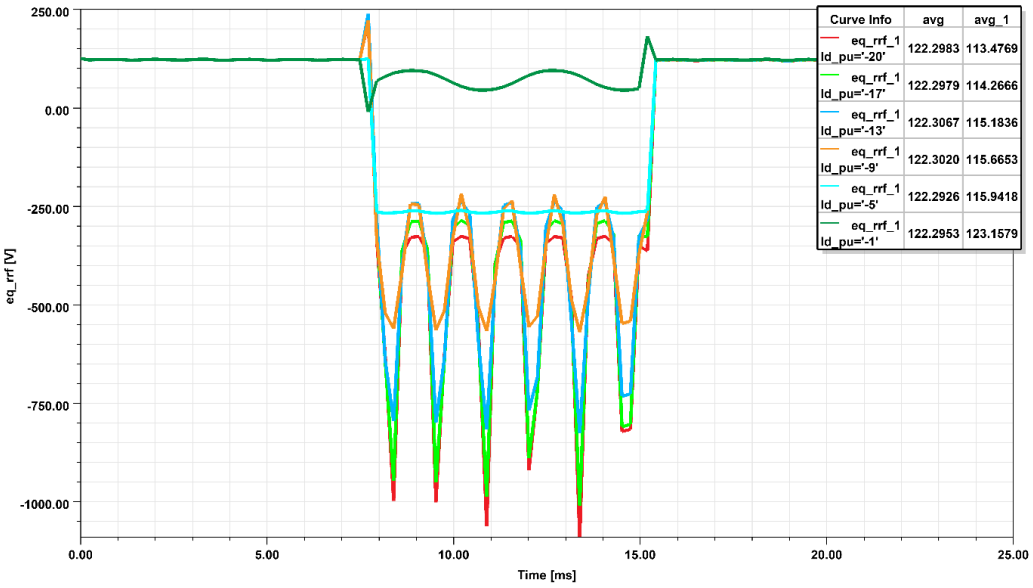

(c)

Figure 8 Time dependent variation of Eq voltages obtained at different I_{s_pu} levels. a-) for 80C magnet b-) for 120C magnet c-) for 150C magnet

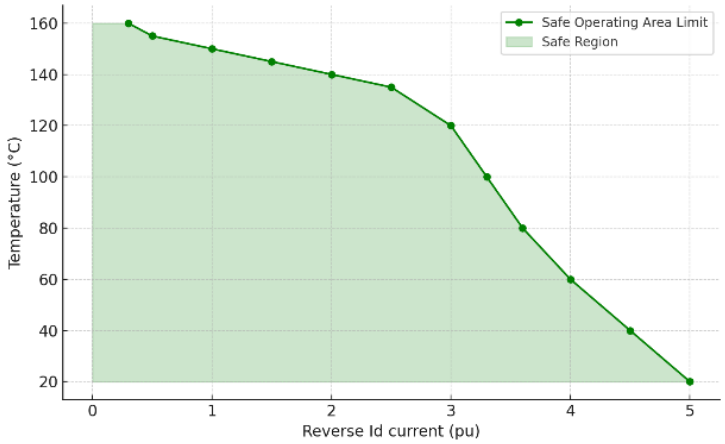

Figure 9 Safe operating area

Additionally, the resulting graphs demonstrate that with increasing temperature, the magnet becomes demagnetized at lower reverse current levels. As a result of these analyses, a Safe Operating Area (SOA) graph was obtained, which determines the safe operating limits in terms of motor design, as shown in Figure 9. The area under the graph represents the safe operating area without the risk of demagnetization. This graph allows a more accurate selection of the magnet class to be used in PMLSM design.

4. Conclusions

In this study, the demagnetization tendencies of permanent magnets in a PMLSM under overload and temperature rise conditions were evaluated through both the BH curve and the E_q voltage. The results indicate that as the temperature increases, PM experience irreversible magnetic losses at lower reverse current levels. The comparison between E_{q1} and E_{q3} emerges as a simple yet effective method for detecting demagnetization. Furthermore, the progression of the operating points on the BH curve directly reveals

whether the magnet has fallen below its "knee point". Through this PMLSM-specific design study, the critical thresholds for magnets under temperature rise due to motor operation and potential short-circuit current scenarios were identified, and a corresponding SOA diagram was established. Future research can focus on the optimization of the MMF value and magnet sizing to ensure safer and more efficient operation of the motor. In future research, we will combine the developed mathematical model of the PMLSM developed in Ansys with the optimization algorithm. Next, the optimization will be carried out.

Declaration of Ethical Standards

As the authors of this study, we declare that he complies with all ethical standards.

Credit Authorship Contribution Statement

E.Yucel: Conceptualization, Methodology, Software, Validation, Formal analysis, Writing -Original Draft, Visualization.
M. Çunkaş: Investigation, Resources, Writing, Review & Editing, Supervision, Funding acquisition.
Ł. Knypiński: Writing, Review & Editing.

Declaration of Competing Interest

The authors declared that they have no conflict of interest.

Funding / Acknowledgements

The authors were supported within the scope of the research by the Selcuk University Scientific Research Projects Unit with Project No: 24111004.

Data Availability

No datasets were generated or analyzed during the current study.

References

Almandoz, G., Gómez, I., Ugalde, G., Poza, J., & Escalada, A. J. (2019). Study of demagnetization risk in PM machines. *IEEE Transactions on Industry Applications, 55*(4), 3490-3500.

Campbell, P. (1996). Permanent magnet materials and their application.

Eker, M., & Özsoy, M. (2022). Effect of demagnetization faults on line start AF-PMSM performance. *Journal of Power Electronics, 22*(6), 1001-1009.

Gyftakis, K. N., Ab Rasid, S., Skarmoutsos, G. A., & Mueller, M. (2021). The demagnetization harmonics generation mechanism in permanent magnet machines with concentrated windings. *IEEE Transactions on Energy Conversion, 36*(4), 2934-2944.

Hanselman, D. C. (2003). *Brushless permanent magnet motor design*: The Writers' Collective.

Hoang, D.-T., Nguyen, M.-D., Kim, S.-M., Bang, T.-K., Kim, Y.-J., Shin, K.-H., & Choi, J.-Y. (2024). Irreversible Demagnetization Prediction Due to Overload and High-Temperature Conditions in PMSM Based on Nonlinear Analytical Model. *IEEE Transactions on Energy Conversion*.

Mahmouditabar, F., Vahedi, A., & Marignetti, F. (2023). The demagnetization phenomenon in PM machines: principles, modeling, and design considerations. *IEEE Access, 11*, 47750-47773.

Song, J., Dong, F., Zhao, J., Lu, S., Dou, S., & Wang, H. (2017). Optimal design of permanent magnet linear synchronous motors based on Taguchi method. *IET Electric Power Applications, 11*(1), 41-48.

Üstün, Ö. (2000). Sürekli Mıknatıslı Baskılı Devre Endüvili Doğrusal Fırçasız Doğru Akım Motoru Tasarımı.

Wang, H., Li, J., Qu, R., Lai, J., Huang, H., & Liu, H. (2018). Study on high efficiency permanent magnet linear synchronous motor for maglev. *IEEE Transactions on Applied Superconductivity, 28*(3), 1-5.

Wang, S., Chen, J., Yang, J., Zhang, C., Qiu, S., Liu, K., & Lyu, B. (2025). Analysis of Temperature Rise in Short-Term High Overload Torque Motor with LPTN Considering Demagnetization and Saturation. *IEEE Transactions on Energy Conversion*.

Xiong, H., Zhang, J., Degner, M. W., Rong, C., Liang, F., & Li, W. (2016). Permanent-magnet demagnetization design and validation. *IEEE Transactions on Industry Applications, 52*(4), 2961-2970.

Yang, D,. Feng, H., Zhang, W., Zhang, H., & Xu, X. (2023). Design and Optimization of Permanent Magnet Linear Synchronous Motor for Direct Drive Multi-car Elevator Variable Rail System. *IEEE Transportation Electrification Conference and Expo,* Chiang Mai, Thailand, 28 November 2023 - 01 December 2023.